IOPscience iopscience.iop.org

Home Search Collections Journals About Contact us My IOPscience

Collisionless ion drag force on a spherical grain

This article has been downloaded from IOPscience. Please scroll down to see the full text article.

2006 Plasma Phys. Control. Fusion 48 185

(http://iopscience.iop.org/0741-3335/48/2/002)

View the table of contents for this issue, or go to the journal homepage for more

Download details:
IP Address: 198.125.179.168
The article was downloaded on 01/02/2012 at 19:05

Please note that terms and conditions apply.

INSTITUTE OF PHYSICS PUBLISHING PLASMA PHYSICS AND CONTROLLED FUSION

Plasma Phys. Control. Fusion **48** (2006) 185–202 doi:10.1088/0741-3335/48/2/002

Collisionless ion drag force on a spherical grain

I H Hutchinson

Plasma Science and Fusion Center, Massachusetts Institute of Technology, Cambridge, MA, USA

Received 18 August 2005, in final form 2 November 2005
Published 4 January 2006
Online at stacks.iop.org/PPCF/48/185

Abstract

The ion drag force on a spherical grain situated in a flowing collisionless plasma is obtained from the specialized coordinate electrostatic particle and thermals in cell simulation code (SCEPTIC) (Hutchinson 2002 *Plasma Phys. Control. Fusion* **44** 1953, Hutchinson 2003 *Plasma Phys. Control. Fusion* **45** 1477, Hutchinson 2005 *Plasma Phys. Control. Fusion* **47** 71) and compared with recent analytic approximate treatments in the interesting and relevant case when the Debye length is only moderately larger than the sphere radius. There is a substantial complex structure in the results for transonic flows, which is explained in terms of the details of ion orbits. Naturally the prior analytic approximations miss this structure, and as a result they seriously underestimate the drag for speeds near the sound speed. An easy-to-evaluate expression for force is provided that fits the comprehensive results of the code. This expression, with minor modification, also fits the results even for Debye length much smaller than the sphere radius.

(Some figures in this article are in colour only in the electronic version)

1. Introduction

The problem of the drag of ions upon a spherical charged dust grain, when there is a relative velocity between the plasma ions and grain, has received much renewed attention recently. Accurate theoretical values for this force are important for understanding the dynamics of dusty plasmas, but have not previously been available in all regimes of interest, even for completely collisionless ions. In the limit when the Debye length ($\lambda_{De} \equiv (\epsilon_0 T_e/e^2 n_e)^{1/2}$) is very large compared with the radius of the grain or particle (r_p), the problem reduces to the classic problem of Coulomb collisions, which was first studied by Chandrasekhar in the context of stellar collisions [4]. The classic solution depends upon the ratio λ_{De}/b_{90} being large, which allows one to approximate the near potential as that of an unshielded charge cut off at the Debye length. (Here $b_{90} = q_1 q_2/4\pi\epsilon_0 m_r v^2$ is the 90° scattering impact parameter for Coulomb collisions, with q_1, q_2 as the charges, m_r the reduced mass and v the initial relative particle velocity.) In integrations over a distribution of velocities, the argument of the Coulomb logarithm, $\ln\Lambda = \ln\lambda_{De}/b_{90}$, can be then taken as constant and given a 'typical' value without introducing a large fractional error in the drag.

 © 2006 IOP Publishing Ltd Printed in the UK

Since the usual definition of a plasma includes the condition that the number of particles in the Debye sphere, $(4\pi/3)\lambda_{De}^3 n_e$, should be large, and since it is an elementary identity that for particles possessing one electronic charge $(4\pi/3)\lambda_{De}^3 n_e = \lambda_{De}/3b_{90}$ (using a typical thermal velocity such that $mv^2 = ZT_e$), elementary particles in normal plasmas always have a large Coulomb logarithm argument. (The so-called 'strongly coupled plasmas' are the exception but are abnormal). Therefore the classic solution is well founded for atomic particles.

However, for a floating grain of finite radius, b_{90} is generally at least as large as approximately r_p. Dust grains may have radii that are not a very small fraction of the Debye length. In that case, their charge is so large that the Coulomb logarithm is of the order unity, and the classic solution approximations break down. Moreover, a dust particle, unlike an elementary particle, absorbs ions impinging on its surface. (More precisely it neutralizes them so that if they are re-emitted, it is as neutrals, relatively decoupled from the rest of the plasma.) Ion absorption owing to the finite radius of the grain gives rise to modifications of the ion drag force.

Additional complications arise because the shielding of the potential around a dust grain must include the effect of ions. For stationary plasma (relative to the grain) the 'linearized' form for the total shielding length $1/\lambda_s^2 = 1/\lambda_{De}^2 + 1/\lambda_{Di}^2$ is an appropriate approximation. And when T_i/ZT_e $(= \lambda_{Di}^2/\lambda_{De}^2)$ is small, as it often is in dusty plasmas, the resulting shielding length is considerably shorter than λ_{De}. But the flow of order of the ion thermal velocity or greater invalidates the 'linearized' shielding approximation. In addition to a reduction of the shielding effect of ions, there arise complicated asymmetric distributions of ion charge around the the grain, which give rise to a potential that is not well represented by any symmetric form, let alone the 'linearized' Debye–Hückel solution for potential $\phi(r) = q_1 \exp(-r/\lambda_s)/4\pi\epsilon_0 r$. The Debye–Hückel form is inaccurate in any case close to the grain, since it requires $|\phi| \ll T_e/e$, which is essentially always violated for a floating grain. All of these difficulties become serious when the Coulomb logarithm is not large, because the effect of the resultant uncertainties in its argument cannot then be ignored as they generally are for plasma particle collisions.

Analytical theories of the ion drag force generally proceed by attempting to extend the Chandrasekhar approach to include ion absorption and to the case of small Coulomb logarithm. The effect of ion absorption can reasonably be addressed [5–7] by splitting the drag into two parts, one (F_c) attributable to the direct collection of momentum for ions that collide with the grain, and the other (F_o) attributable to ions that orbit the grain, without being collected. If the potential can be treated as spherically symmetric and $\lambda_{De}/r_p > 1$, then the orbital motion limited (OML) treatment [8] is justified. In that case the marginal impact parameter for ion collection (b_c) is given by $b_c^2 = r_p^2[1 - Ze\phi_p/(\frac{1}{2}m_i v^2)]$, where ϕ_p is the potential of the particle (grain) and Ze the ion charge. The OML ion collection drag force for a Maxwellian ion distribution shifted by a flow velocity v_f may be expressed [3, 9] in terms of $u = v_f/v_{ti}$, normalized to an ion thermal velocity $v_{ti} = \sqrt{2T_i/m_i}$ as

$$F_c = n_i r_p^2 m_i v_{ti}^2 \frac{\sqrt{\pi}}{2}\left\{u(2u^2+1+2\chi)e^{-u^2} + \left[4u^4+4u^2-1-2(1-2u^2)\chi\right]\frac{\sqrt{\pi}}{2}\mathrm{erf}(u)\right\}/u^2, \tag{1}$$

where $\chi \equiv -Ze\phi_p/T_i$ is the normalized potential.

The orbital part of the force may conveniently be written in the form that arises from the usual cut-off Coulomb potential calculation:

$$F_o = n_i \frac{q_i^2\phi_p^2}{m_i v_{ti}^2} r_p^2 8\pi\ G(u)\ \ln\Lambda, \tag{2}$$

where the Chandrasekhar function, $G(u) \equiv [\mathrm{erf}(u) - 2ue^{-u^2}/\sqrt{\pi}]/(2u^2)$, takes proper account of the finite flow velocities, not just the limit $u \ll 1$ where $G(u) \to 2u/(3\sqrt{\pi})$. However,

this form has just formally concentrated all of the uncertainties of the treatment into the value of $\ln \Lambda$, which now must be considered to be a function of flow velocity (as well as particle radius and plasma parameters). The main advantage of the form is that it naturally embodies the classic solution for large Λ. The force F_o (not to mention b_{90}) is more usually expressed in terms not of the particle potential but of the particle charge q_p. In the limit of large Λ, a simple identity relates them: $q_p = 4\pi\epsilon_0\phi_p r_p$. However, when finite λ_s is taken into account, the relationship is more ambiguous: in F_o and b_{90} do we put $q_p = 4\pi\epsilon_0\phi_p r_p \exp(r_p/\lambda_s)$ (matching the Yukawa potential form to the surface potential), or $q_p = 4\pi\epsilon_0\phi_p r_p(1 + r_p/\lambda_s)$ (matching the product of potential and capacitance), or since we are using a cut-off Coulomb potential approximation, do we retain $q_p = 4\pi\epsilon_0\phi_p r_p$?

A physically plausible extension of the cut-off integral approximation to finite-radius particles [5–7] is to apply the lower impact parameter cut-off not at b_{90} but at b_c. In this approach

$$\ln \Lambda = \frac{1}{2} \ln \left[\frac{b_{90}^2 + \lambda_s^2}{b_{90}^2 + b_c^2} \right]. \tag{3}$$

This expression has a correct asymptotic form for large λ_s but clearly breaks down near $\lambda_s \sim b_c$, since for $\lambda_s < b_c$ it becomes negative. (In subsequent plots we then set $\ln \Lambda = 0$.)

A different form has been proposed by Khrapak and co-workers [10–12], motivated by the argument that the upper impact-parameter-integral cut-off should be when the distance of the closest approach (not the impact parameter itself) is equal to λ_s. The resulting form is[1]

$$\ln \Lambda = \ln \left[\frac{b_{90} + \lambda_s}{b_{90} + r_p} \right]. \tag{4}$$

This form gives much better numerical agreement with the drag force based on integrals over the momentum loss cross-section for a Yukawa potential [13, 14] (when the particle radius is taken as negligible) and therefore has greater plausibility as a small-λ_s approximation.

The compact forms of these equations are convenient, but they mask a number of uncertainties, notably

- What should one take for an exact relationship of $r_p\phi_p 4\pi\epsilon_0$ to the particle charge q_p?
- What value to take for λ_s?
- What velocity or energy to substitute in b_{90} and b_c?

These uncertainties are not fully resolved even for the large-Λ solutions that are standard in plasma collisions; but for that case, it does not practically matter, since the error introduced is of the order $1/\Lambda$ for the charge/potential ambiguity and for the others logarithmically small. For dust drag, however, with $\Lambda \sim 1$, no such mitigating factor intervenes. It is essential to resolve these uncertainties before accuracy can be obtained.

In view of the various approximations of uncertain accuracy associated with these analytical approaches, confrontation with full numerical calculations incorporating exact treatments of the problem seem essential. They are now also possible because a particle in cell code named specialized coordinate electrostatic particle and thermals in cell (SCEPTIC) has recently been developed. It is described in detail in a series of papers [1–3]. It solves the full non-linear, asymmetric-potential, electrostatic, collisionless kinetic theory problem, by integrating ion orbits in a six-dimensional phase space, in the self-consistent potential having rotational symmetry only about the direction of plasma flow, on a spherical mesh, with thermal (Boltzmann) electron density. The number of particles used (typically about seven million) is sufficient to allow the drag force to be obtained quite accurately for flow velocity from subsonic

[1] Reference [3] contained typographical errors, accidentally writing b_c for r_p in its equation (9) and the succeeding text.

to supersonic. And it makes none of the approximations of the analytic theories. It is however limited to modest ratios of λ_{De}/r_p: up to about 20 for good accuracy, because of the finite domain over which the calculations are done, limited by computational resources. However, this low-Λ region is precisely where the limitations of the analytic theories are most severe. For higher values the analytic approximations are good; they all agree with each other; and the need for correcting them with exact calculations is less.

This paper presents a critical comparison of the results of SCEPTIC with the analytical approximations. It shows that, contrary to some prior implications, the Khrapak form with natural values for λ_s and b_{90} does not give accurate values for the drag in small-Λ cases when the drift substantially exceeds the ion thermal speed. The analytic calculations underestimate the drag by up to a factor of 2. The reasons for this discrepancy and for the associated significant structure in the drag force variation with velocity are explained by a detailed analysis of the SCEPTIC results and the associated ion orbits. The results of a wide range of code calculations are fitted with a modified form of $\ln\Lambda$, which allows convenient evaluation over the whole range of parameters and gives correctly the asymptotic limits. The ambiguities in λ_s and b_{90} are resolved, numerically at least, and the uncertainties associated with linearization, etc completely avoided.

The present work extends the earlier initial observations of ion force in SCEPTIC [3] notably in that it includes ion temperatures as low as $0.01ZT_e$, which are important in laboratory dusty plasmas. A brief preliminary outline of the present SCEPTIC results was presented in [15].

2. SCEPTIC calculations

For a full description of the code, [1–3] should be consulted. In brief, SCEPTIC solves self-consistently the following equations. Each ion, of charge Ze and mass m_i, at position $\boldsymbol{x}$ is governed by the equation of motion in the electrostatic potential:

$$m_i \frac{d^2\boldsymbol{x}}{dt^2} = -Ze\nabla\phi. \tag{5}$$

The electrons are taken to have the density

$$n_e = Zn_{i\infty}\exp(e\phi/T_e), \tag{6}$$

where $n_{i\infty}$ is the ion density where $\phi = 0$, far from the probe.

The self-consistent potential satisfies Poisson's equation:

$$\nabla^2\phi = \frac{e}{\epsilon_0}(n_e - Zn_i), \tag{7}$$

where the ion density n_i is obtained by integration over all velocities of the ion distribution function, $f(\boldsymbol{x}, \boldsymbol{v})$ which is represented by the large number of individual ions in the calculation. Ions leaving the computational domain, which extends from the grain's spherical surface to an appropriately chosen outer spherical boundary, are re-injected from the outer boundary with statistics chosen to represent a shifted Maxwellian distribution at infinity.

In this paper only equipotential (conducting) grains are considered. Their potential satisfies the floating condition, which, in the OML approximation, is the solution of

$$\begin{aligned}\overline{\Gamma_e}(\phi_p) &= \frac{1}{4}n_{e\infty}\left(\frac{8T_e}{\pi m_e}\right)^{1/2}\exp(e\phi_p/T_e)\\ &= Z\overline{\Gamma_i} = n_{e\infty}v_{ti}\frac{u}{4}\left\{\left(1+\frac{1}{2u^2}+\frac{\chi}{u^2}\right)\mathrm{erf}(u)+\frac{1}{u\sqrt{\pi}}\exp(-u^2)\right\}.\end{aligned} \tag{8}$$

It has been shown using SCEPTIC that this result is in excellent agreement with the potential based on the actual self-consistent ion collection, when $\lambda_{De} > r_p$, and it proves advantageous in this regime to stability and convergence at a low ion temperature to run the code with fixed sphere potential. At lower λ_{De} SCEPTIC is run obtaining the floating potential directly from its own ion flux.

The SCEPTIC runs undertaken here are more demanding than those previously reported because they are in the upper range of the domain size (up to 40 times the particle radius) feasible with the present implementation. It has been found that a domain radius at least twice λ_{De} is needed to avoid distortion of the force results by the approximate nature of the boundary conditions. We explore down to $T_i = 0.01ZT_e$, at which value the thermal ion velocity is very small. So it takes a thermal ion a far longer time to traverse the computational domain, and thus the simulations must be run for a longer time before convergence is obtained. Typically 2000 timesteps of length up to $0.15r_p/c_s$ each are used ($c_s \equiv \sqrt{ZT_e/m_i}$). Subcycling of the orbit integrations within these timesteps is used at positions close to the probe, to ensure accuracy in regions of large gradients. Low T_i also leads to low ion Landau damping; and oscillations in the form of sound waves need this long time duration (>4 sound-wave transits of the domain) to damp away and thus give a converged result. No cases of unequivocal unsteady asymptotic flow states have been observed, but recall that rotational symmetry about the external flow direction is imposed. The potential mesh has 100×100 cells, equally spaced in r and in the cosine of the polar angle, $-1 \leqslant \cos\theta \leqslant 1$.

The drag force consists locally of three (stresses or) momentum flux densities, integrated over an arbitrary sphere surrounding the particle: (1) the ion momentum flux, (2) the electron pressure and (3) the Maxwell stress arising from the electric field. The fraction of the force attributable to each of these components varies as a function of the sphere radius chosen. Note that division into these local components, while physically indisputable, is *not* the same as the conceptual division into contributions at infinity from collected and orbiting particles used by the analytic theories. The total force is independent of the radius of the sphere of integration in steady state: a reflection of the conservation of momentum and a useful test of code accuracy and convergence.

Figure 1 shows an example comparing the force components at the grain surface (black solid curves) with those at the domain boundary (red dotted curves), as a function of flow velocity. Focusing first on the hollow squares, which show the total force (momentum flux), the agreement between the values at the two surfaces is a measure of the accuracy and the extent of convergence of the code results. The largest discrepancies amount to only about 5% of the peak force. However, since the absolute discrepancy is almost independent of velocity, the fractional error becomes increasingly important at low velocities, where the force tends linearly to zero. The electric field force, arising from the Maxwell stress (triangles), is negligible at the outer boundary but very substantial for the grain surface. Indeed, the entire drag force on the grain can be considered to be transmitted at its surface by a combination of ion momentum flux and the Maxwell stress, since the electron pressure force (filled circles) is zero at the grain because it is an equipotential and the electron pressure is governed by potential through the Boltzmann approximation. The electron pressure asymmetry is rather significant at the outer boundary and changes sign as flow velocity changes. The ion momentum flux to the grain (filled squares) shows a remarkable transition from negative to positive at a flow velocity of about $0.6\sqrt{ZT_e/m_i}$. The transition is only partly compensated by changes in the electric field force, and so a sharp upward rise in the total drag force occurs. In the vicinity of the transition, the extreme sensitivity of the force is part of an overall sensitivity of the system to small perturbations. The simulation is very slow to converge at these parameters, which is one reason for the large total force discrepancy for $v_f = 0.6\sqrt{ZT_e/m_i}$.

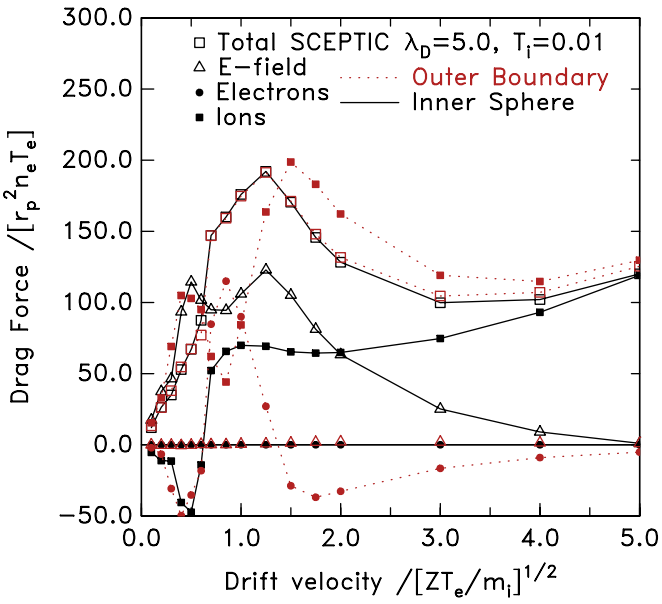

Figure 1. Decomposition of the force components from SCEPTIC on a floating particle. ($\lambda_{De} = 5r_p$, $T_i = 0.01ZT_e$, $m_i/Z = 40m_{proton}$: Ar^+).

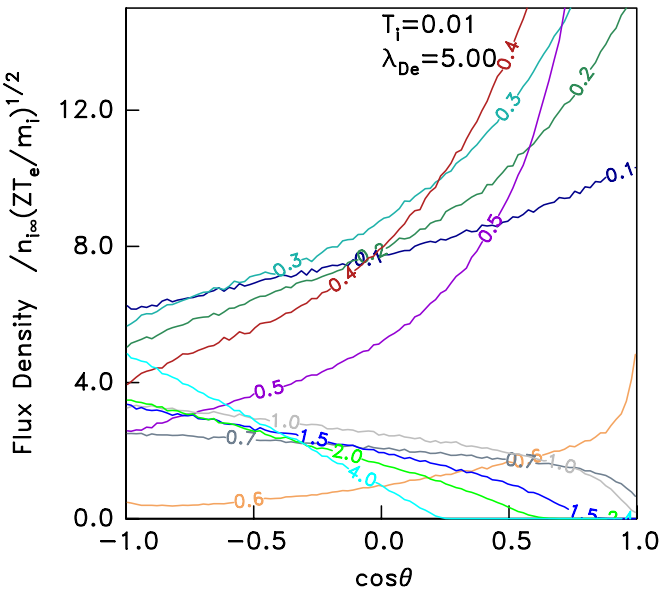

Figure 2. Ion flux density as a function of angular position on a floating particle. The plasma flow velocity in units of $\sqrt{ZT_e/m_i}$ labels each curve. ($\lambda_{De} = 5r_p$, $T_i = 0.01ZT_e$, $m_i/Z = 40m_{proton}$: Ar^+).

This transition in force is associated with an even more dramatic transition in the collected ion flux distribution, which is shown in figure 2. As has been noted before [2], in some conditions (including those under consideration here) a remarkable reversal of the asymmetry of the ion collection flux density occurs. The downstream side of the probe ($\cos\theta > 0$)

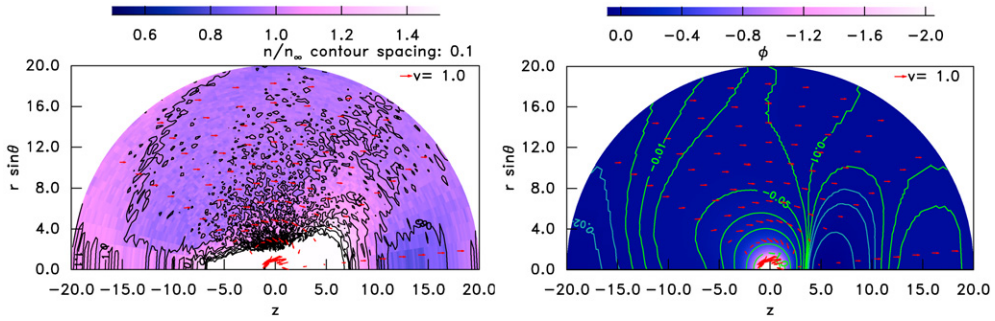

Figure 3. Density and potential contours when $v_f = 0.5c_s$, showing an elongated high density near the grain both upstream and downstream, a modest density rise upstream far from the grain, and a very weak oscillation in the wake.

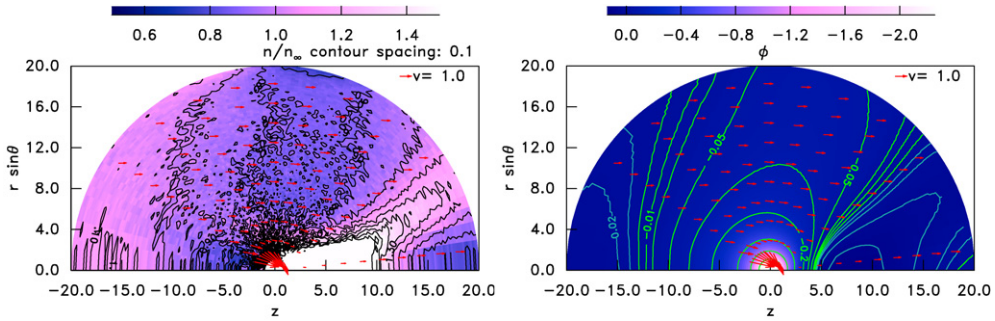

Figure 4. Density and potential contours when $v_f = 0.7c_s$, showing that high density just upstream of the probe has disappeared and the wake is elongated.

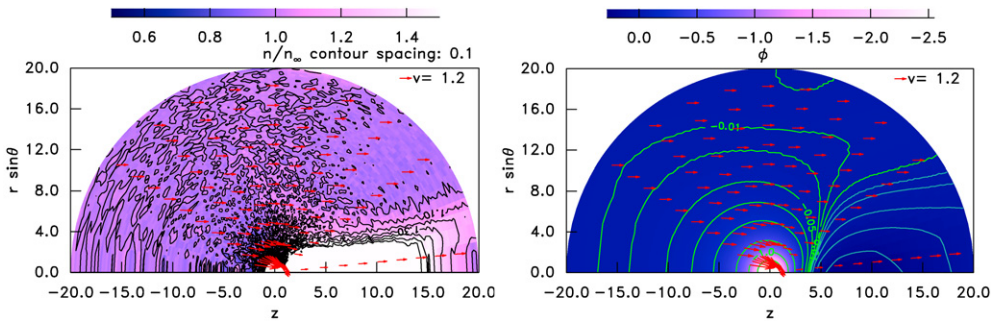

Figure 5. Density and potential contours when $v_f = 1.25c_s$, showing negligible upstream density perturbation and a long high-density wake.

collects more than the upstream side. This phenomenon is evident in the figure for flow velocity $v_f \leqslant 0.5$ ($\times\sqrt{ZT_e/m_i}$). However, this asymmetry reversal disappears for $v_f \geqslant 0.7$. Notice that the curve for $v_f = 0.6$ is far from those of either of its adjacent flow velocities. It is this transition that is causing the change in sign of the ion momentum collection.

In figures 3–5 contours of the density and potential profiles associated with the transition of the ion collection are shown. For all of these, $\lambda_{De} = 5r_p$, $T_i = 0.01ZT_e$ and $m_i/Z = m_{proton}$, though the results are qualitatively the same for $m_i/Z = 40m_{proton}$. They show that the

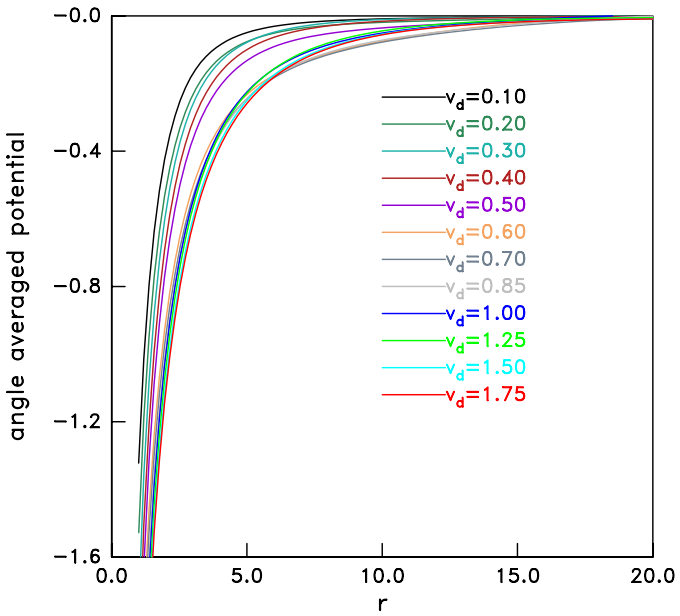

Figure 6. Profiles of angle-averaged potential (in units of T_e/e) versus radius (normalized to r_p) for different flow velocities. ($\lambda_{De} = 5r_p$, $T_i = 0.01ZT_e$ and $m_i/Z = m_{proton}$).

transition occurs as the shielding cloud of ions effectively disappears from immediately upstream of the grain. At a slightly higher flow velocity ($>0.7c_s$), the modest density enhancement upstream from the grain, that was previously present, also disappears.

Figure 6 shows the corresponding profiles of the potential averaged over angle θ. The transition in ion collection and force accompanies a sudden drop in the average potential around the grain at $v_f = 0.6c_s$, which corresponds to the stripping away of the ion shielding from upstream of the grain.

The density is obviously very asymmetric at higher velocities. The potential is less asymmetric, but the question arises as to how important the potential asymmetry is. This can be answered by running SCEPTIC in a mode where the potential is artificially symmetrized by angle averaging, at each step before calculating the ion force. The result of this unphysical process, which models the effect of a theoretical potential symmetry assumption, shows a comparable evolution of the average potential with v_f except that the decrease of the potential is far more gradual. It does not take nearly so sudden a drop at the transition velocity ($v_f = 0.6c_s$). Thus potential asymmetry is very important in enhancing the suddenness of the transition, but the qualitative evolution of the ion shielding cloud passes through the same stages even without potential asymmetry.

A more fundamental understanding of the reasons behind these effects can be gained by examining the individual particle orbits. In figure 7 the examples are shown. Since the ion thermal velocity is low, these orbits are all for ions that impinge at exactly the drift velocity. Also we use angle-averaged potential, in order to make it possible to follow the orbits with a simple angle integration. Therefore these orbits are to be regarded as illustrative, but they explain the key features just noted.

At velocities below the transition, there exist many orbits that circle considerably more than 360° around the grain, before returning to infinity. The existence of such orbits also implies that there are orbits that circle more than 180° around the grain before colliding with

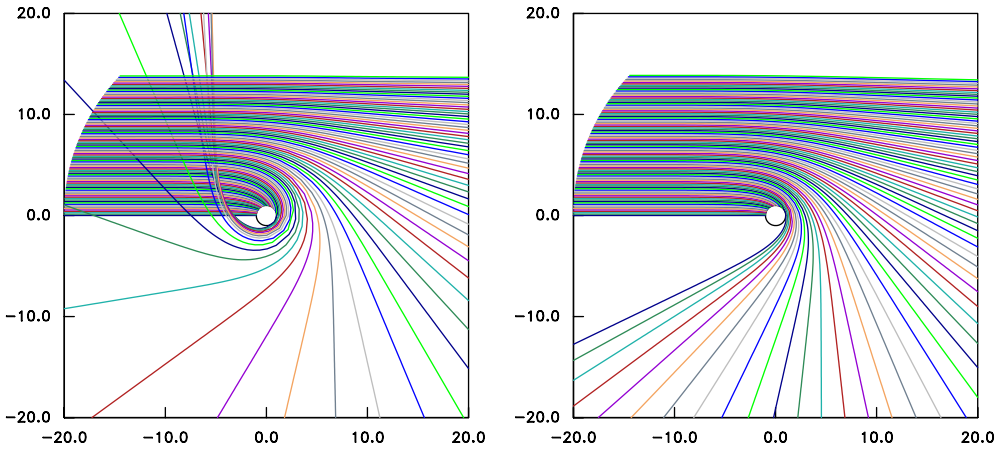

Figure 7. Typical orbits when the flow velocity is $v_f = 0.5c_s$ (below the transition, left) and $v_f = 0.8c_s$ (above the transition, right).

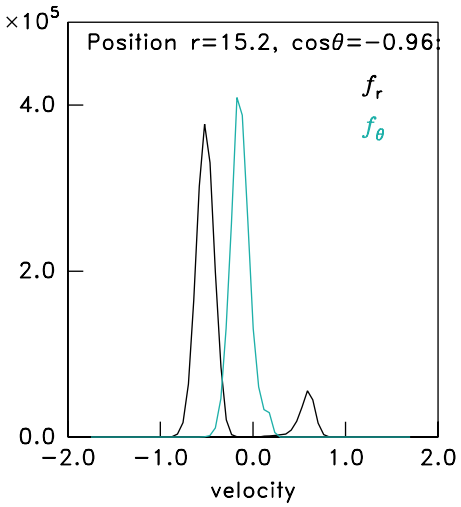

Figure 8. Ion distribution close to the axis far upstream of the particle: $r = 15.2r_p$, $\cos\theta = -0.96$. The radial and angular velocity distributions are f_r and f_θ, showing the second stream arising from ions on returning orbits. ($\lambda_{De} = 5$, $T_i = 0.01ZT_e$, $v_f = 0.5$, $m/Z = m_{proton}$. Units of f are particle count in cell, summed over 40 timesteps.)

its surface. Above the transition, these orbits do not exist. Whether or not these orbits exist controls whether or not there is an enhanced ion density immediately upstream of the grain, contributing to potential shielding. This will be the case only if $>360^\circ$ orbits exist. Next it controls, at a minimum, whether there will be an overlap of the regions on the downstream surface of the grain where ions are collected from both sides of the grain. This occurs if and only if there are collected orbits that extend to more than 180°. The last effect to disappear, at velocities slightly higher than the transition, is the presence of marginal orbits that circle approximately 360°, and are thus sling-shotted back upstream, causing enhancement of the density there by the observed second ion stream, far from the grain. Figure 8 shows the ion distribution function far upstream, confirming this interpretation. Thus, consideration of

Table 1. Conventions adopted for evaluating key parameters.

Parameters	Known asymptotes $v_f \ll v_{ti}$	Known asymptotes $v_f \gg v_{ti}$ (or c_s[†])	Interpolating expression
b_{90}/r_p	$Ze\lvert\phi_p\rvert/2T_i$	$Ze\lvert\phi_p\rvert/m_i v_f^2$	$Ze\lvert\phi_p\rvert/(2T_i + m_i v_f^2)$
$\lambda_s^2 - \lambda_0^2$	$\lambda_{De}^2/[1 + ZT_e/T_i]$	λ_{De}^2 [†]	$\lambda_{De}^2/[1 + ZT_e/(T_i + m_i v_f^2)]$
b_c^2	$r_p^2[1 - 2Ze\phi_p/2T_i]$	$r_p^2[1 - 2Ze\phi_p/m_i v_f^2]$	$r_p^2[1 - 2Ze\phi_p/(2T_i + m_i v_f^2)]$

the evolution of the populated orbits enables one intuitively to understand essentially all of the main characteristics of the transition and the associated changes in the plasma vicinity. In particular, it shows why the transition simultaneously removes the reversal of the ion collection flux asymmetry and the upstream ion shielding cloud. Both these effects contribute to the rapid rise in the ion drag force.

3. Drag force comparison with analytic approximations

Before making a comprehensive comparison of SCEPTIC's force results with analytic approximations, it is essential to establish conventions to remove the ambiguity in the analytic expressions for q_p, b_{90} and λ_s. We start by specifying that in all expressions, we will use $q_p = r_p\phi_p 4\pi\epsilon_0$ for the particle charge. This choice is not the most accurate estimate for the actual charge on the particle. But it ensures that the Coulomb approximation ($q_p/4\pi\epsilon_0 r$) to the potential is equal to the actual particle potential at its surface and is closer to the actual potential throughout the plasma region than if we had chosen, e.g. $q_p = 4\pi\epsilon_0\phi_p r_p \exp(r_p/\lambda_s)$ and then used the Coulomb approximation. An even more important factor in this choice is that there is no ambiguity about what to use in b_c: the physics of its derivation dictates that it must be based on the actual particle potential. But the Khrapak form for $\ln\Lambda$ is derived using an algebraic cancellation that takes the cut-off Coulomb potential at the particle equal to ϕ_p. Thus, consistency of the Khrapak form *requires* that the charge be chosen this way.

In table 1 the conventions adopted here for analytic comparisons using equations (1)–(4) are summarized. The values for b_{90} and b_c are relatively unambiguous in the limits of $v_f \ll v_{ti}$ and $v_f \gg v_{ti}$. The high flow velocity limit is simple, in that it is the expression for a monoenergetic ion beam. The low flow velocity limit is established by noting that we wish to represent an integration of the monoenergetic drag over a Maxwellian distribution with a zero shift, which gives rise [10] to integrals of the form $\int_0^\infty \exp(-x)\ln\Lambda(x)\,dx$, where $x \equiv mv^2/2T_i$. These integrals can be done, giving terms of the form $\exp(z)E_1(z)$, where $E_1(z)$ is the exponential integral function. (Such an expression for the Khrapak form of $\ln\Lambda$ in the case of the vanishing r_p is given in [16].) A fairly rough approximation, but with correct limits, is $\exp(z)\mathrm{E}_1(z) \approx \ln(1 + 1/z)$. (It is correct to 17% accuracy for real positive z [23], but note that for the standard form of $\ln\Lambda$, equation (3), the integrals give complex values of z). If this substitution is made, then the resulting Maxwell-average is just what would be obtained by substituting $x = 1$ into the integrand logarithm's argument. In other words, the relation between the Maxwell-averaged force and the monoenergetic ion force can be shown to be appropriately expressed by substituting T_i (rather than, e.g. $\frac{3}{2}T_i$) for $\frac{1}{2}m_i v^2$. A convenient, but of course not definitive, expression that bridges between the high and low velocity limits is to put in place of $m_i v^2$ the combination $2T_i + m_i v^2$.

For the screening length, λ_s, matters are more ambiguous. At zero drift velocity, for $r_p \ll \lambda_{De}$, a 'linearized' expression for the shielding length, combining ion and electron Debye lengths in the inverse square, is physically justified. At very high v_f ($\gg c_s$), ion shielding will

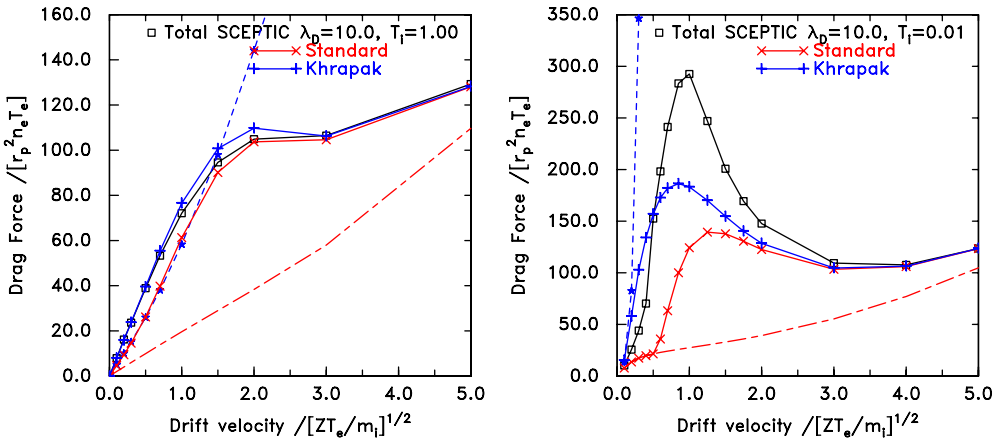

Figure 9. Comparison of analytic approximations: standard (equation (3)) ×; Khrapak (equation (4)) +; low v_f approximation (equation (9)) - ★ -; with the full SCEPTIC calculation: □. The short-long dashed line is the F_c component, the same for all analytic approximations. Here the particle is floating at the OML potential, $m_i/Z = 40m_{proton}$, $\lambda_{De} = 10r_p$.

be negligible. The theoretical results of Daugherty *et al* [17], for monoenergetic, isotropic ion distributions indicate that for zero drift velocity, $\lambda_{De}^2/[1 + ZT_e/m_i v^2]$ is a good approximation. This gives really only a hint at where the transition between the limits takes place. It suggests replacing T_i with $m_i v^2$. Also, in a recent paper, Khrapak *et al* [12], supplementing the binary collision analysis with a linearized response approach following the lines of Peter and Meyer-ter-Vehn [18], propose a model for shielding where, in effect, T_i is replaced in the linearized shielding expression with $T_i + m_i v_f^2$, which seems tolerably to fit their analytic approximate force calculations across the range of flow velocities. Daugherty *et al* [17] have also shown that when r_p/λ_s is not small, the shielding length is greater than the linearized form, which may be accounted for by adding a constant $\lambda_0^2 \sim r_p^2$ to the form for λ_s^2. That effect is not large in this context, and figure 9 sets $\lambda_0 = 0$, but $\lambda_0 = r_p$ will be included later in equation (10) and figure 10, which enforces non-negativity on $\ln\Lambda$. These factors motivate the present comparison choices, but since they are little more than heuristic, no claim is implied that the choices are 'correct'.

A further comparison of interest is that previous authors have often given only low-flow ($v_f \ll v_{ti}$) expressions for the force. For example, the final result in [10] (equation (11)) is an expression equivalent, in the present notation, to

$$F_c + F_o = 8\frac{\sqrt{\pi}}{3} r_p^2 n_i m_i v_{ti} v_f \left[1 + \frac{b_{90}(v_{ti}/\sqrt{2})}{2r_p} + \left(\frac{b_{90}(v_{ti}/\sqrt{2})}{2r_p} \right)^2 \ln\Lambda \right], \tag{9}$$

which may be considered the small argument expansion of the Chandrasekhar function.

Figure 9 illustrates force comparisons at $T_i = ZT_e$ and $T_i = 0.01ZT_e$. The analytic approximations all use exactly the potential of the corresponding SCEPTIC points; so there are no discrepancies attributable to charging and potential differences. The high temperature case shows a gratifying agreement between SCEPTIC and both the full Chandrasekhar function expressions using equations (3) or (4) and the tabulated parameter conventions. The Khrapak form is noticeably better at intermediate velocity. Reasonable values are also obtained from the low-v_f approximation (9) for $v_f < 1.5$. Unfortunately, none of this good agreement is maintained for the low temperature case, which has a much shorter linearized shielding length.

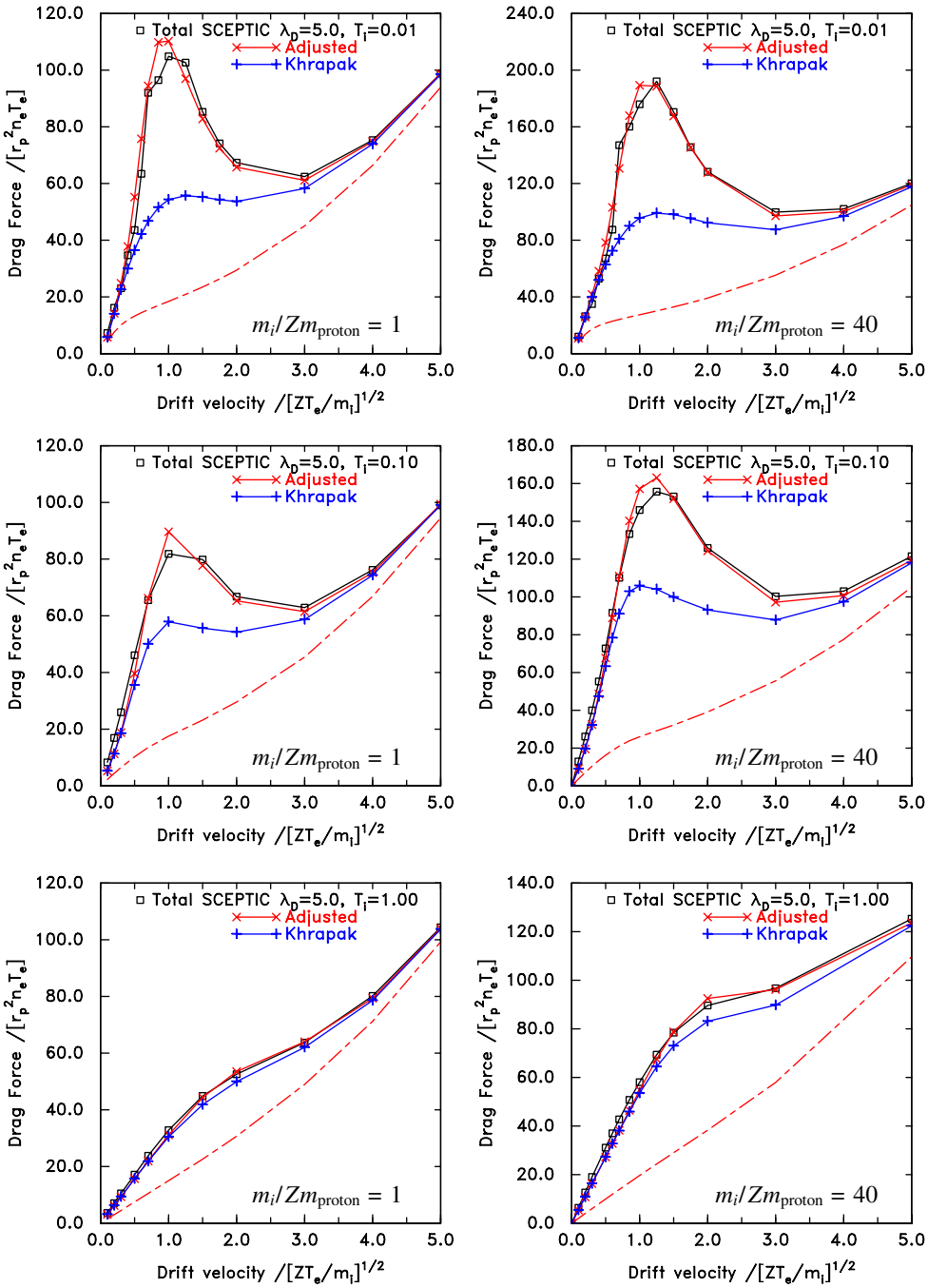

Figure 10. Drag force from SCEPTIC compared with analytic approximations ($\lambda_{De} = 5r_p$).

We see that none of the analytic approximations is convincing. The best is the Khrapak expression, but even that varies from overestimating the force to underestimating it by roughly a factor of 2. The low-v_f approximation greatly overestimates the force for $v_f \gtrsim 0.2$. All the full-form calculations agree at highly supersonic speeds, where the ion shielding disappears.

(It is very difficult to obtain converged SCEPTIC results for $0.2 \leqslant v_f \leqslant 0.4$ in this plot. The values should be treated with caution. They may be in error by up to $15 r_p^2 n_e T_e$.)

In view of the unsatisfactory results from the Khrapak expression, a better approximate analytic expression that fits the numerical results has been developed. It is motivated by the observation that although the Khrapak expression is reasonable in the high and low velocity limits, the reduction of ion shielding as v_f increases is not nearly as gradual as the form of table 1 assumes. As described in the previous section, the shielding is stripped away in an abrupt transition involving the potential asymmetry. Therefore the following form of the parameters λ_s and b_{90} is adopted

$$b_{90} = r_p Ze\phi_p / m_i v_{eff}^2, \qquad \lambda_s^2 = \lambda_{De}^2 / [1 + 2ZT_e / m_i v_{eff}^2] + r_p^2, \tag{10}$$

which enables this transition to be adjusted with an effective velocity, v_{eff}, fitted as

$$m v_{eff}^2 = 2T_i + m_i v_f^2 \left\{ 1 + \left[\frac{v_f / \sqrt{ZT_e / m_i}}{0.6 + 0.05 \ln(m/Z) + (\lambda_{De}/5r_p)(\sqrt{T_i/ZT_e} - 0.1)} \right]^3 \right\}. \tag{11}$$

Here, $m/Z = m_i / m_{proton} Z$, accounts for the effects of the ion mass on the force via the floating potential, and the arithmetic form[2] is chosen for convenience with coefficients fitted to the SCEPTIC results over the ranges $0.01 \leqslant T_i/ZT_e \leqslant 1$, $5 \leqslant \lambda_{De}/r_p \leqslant 20$ and $m/Z = 1,\ 40$.

The form of equation (11) can be considered to give b_{90} and λ_s essentially as before, except that the fractional term provides a rapidly increasing addition to the effective velocity as v_f rises above a threshold determined by the denominator. This increase causes λ_s to tend rapidly to λ_{De} and b_{90} to become small, thus causing the Khrapak expression (which is to be used) for $\ln \Lambda$ to tend to $\ln(\lambda_{De}/r_p)$. At low v_f the fractional term becomes negligible.

In figures 10–12 a gallery of comparisons of this 'adjusted' form (equations (1), (2), (4), (10) and (11)) with the original Khrapak form (using table 1) and SCEPTIC are shown. The adjusted form is a much better fit in all the cases where discrepancies are substantial. The remaining major discrepancy of the adjusted (and Khrapak) form with SCEPTIC is for the cases $\lambda_{De} = 10, 20$, $T_i = 0.01$, $m_i/Z = 40$, in the velocity range $0.2 \leqslant v_f \leqslant 0.4$. Since SCEPTIC convergence is in question there, no form to remove that discrepancy has been developed. The $\lambda_{De} = 20$, $T_i = 1$ cases show SCEPTIC slightly below the analytic forms. This may be caused in part by the limitation of the computational domain size but is probably not outside the uncertainties in the analytic forms.

Since equation (11) applies to b_{90} (as well as λ_s) in Λ, it models a situation in which, above the shielding transition, the drag is actually slightly greater than would be obtained from a standard cut-off based on λ_{De}. The lower limit of the impact-parameter integral, b_{90}, has been artificially reduced. This approach gives a better numerical fit than leaving b_{90} unmodified, but it probably reflects an enhancement of the drag through the asymmetric effects of the potential. I cannot cite a sound heuristic physical reason for the actual reduction of the lower cut-off. This comment emphasizes that the final form, though physically motivated, was not arrived at by heuristic arguments. It seems unlikely that heuristic arguments, such as those that lie behind the analytic forms, could arrive at convincing accurate expressions for the drag force. For that purpose, full-scale calculations such as those of SCEPTIC are indispensable.

4. Short screening length

Dusty plasma parameters such that $\lambda_{De} \lesssim r_p$ are less frequently encountered. Even though probes frequently operate in this regime, the forces on them are of less importance, and they

[2] This form is more consistent and fits slightly better than a similar one given in [15].

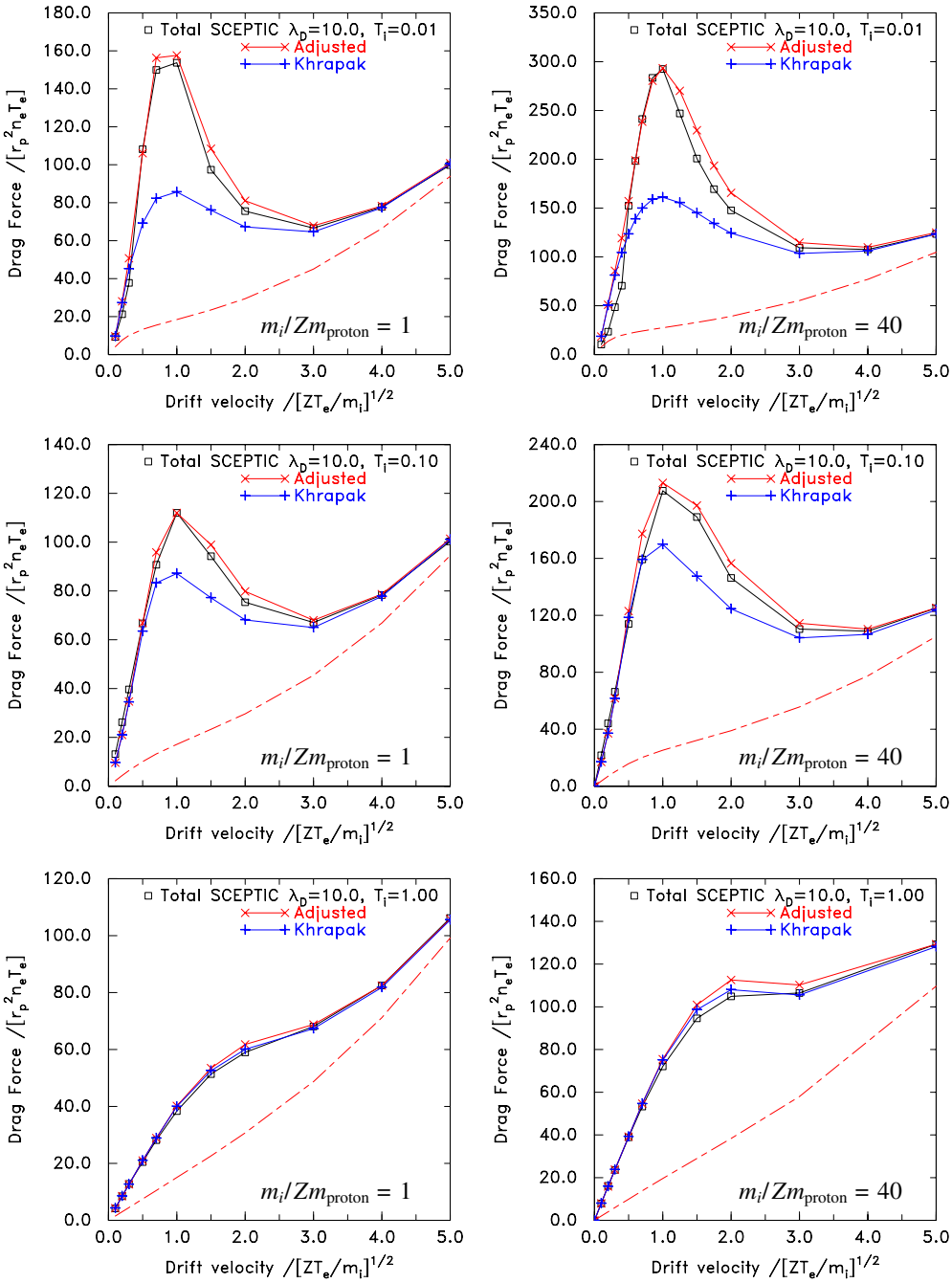

Figure 11. Drag force from SCEPTIC compared with analytic approximations ($\lambda_{De} = 10r_p$).

are not necessarily at floating potential, which is what we are analysing here. Nevertheless, for completeness some results in this regime are presented. Unfortunately SCEPTIC cannot so far avoid unphysical instabilities in this regime when the ion temperature is as low as $0.01ZT_e$ [1]. Therefore we focus on $T_i = 0.1ZT_e$ where numerical problems are absent.

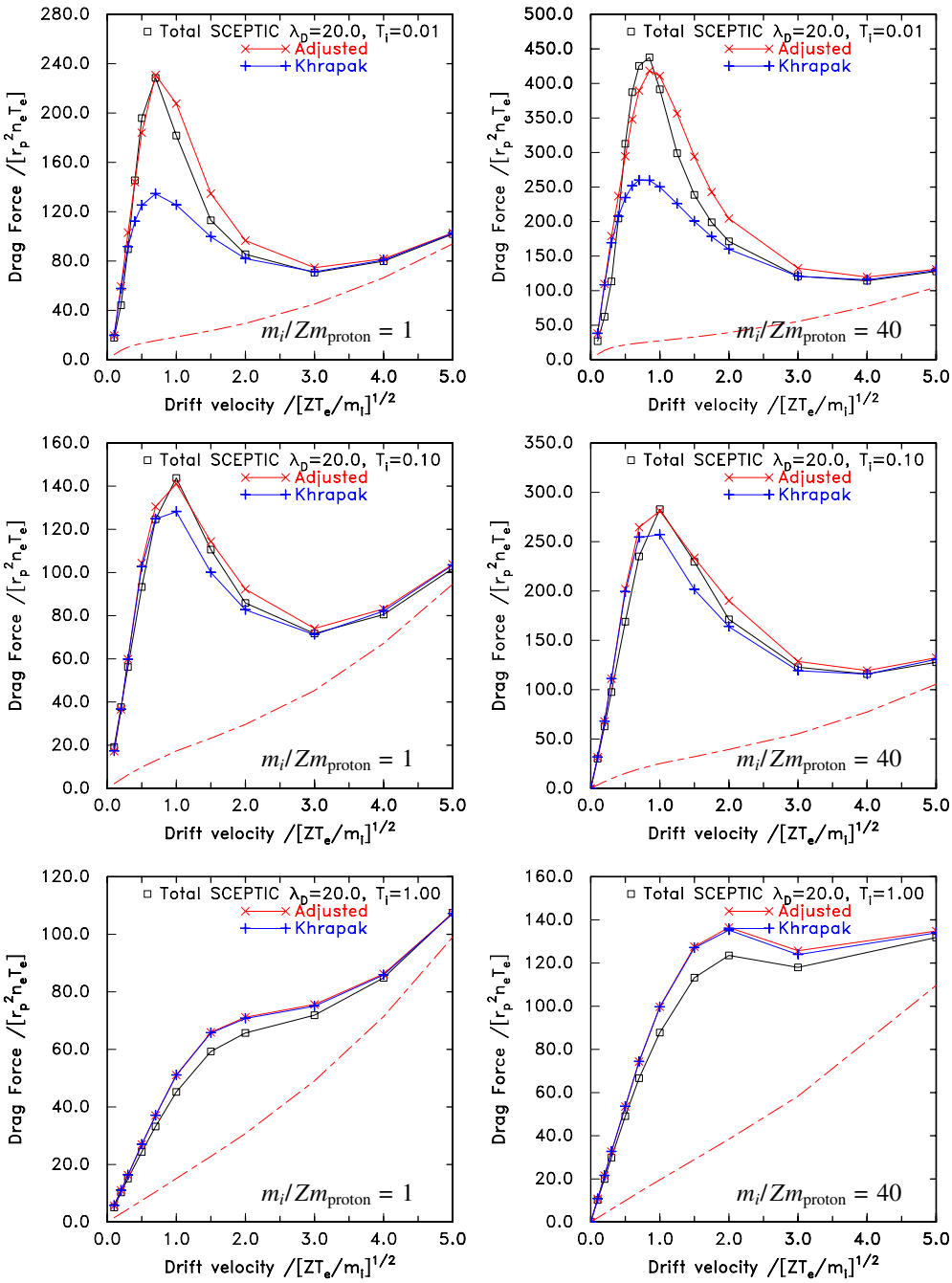

Figure 12. Drag force from SCEPTIC compared with analytic approximations ($\lambda_{De} = 20r_p$).

Figure 13 shows results compared with the analytic forms previously given. Of course the analytic estimates for orbit force have little justification in this regime, and indeed often the Coulomb logarithm would be negative but for our non-negativity constraint. The adjusted formula is low by up to 30% at $\lambda_{De} = 1$. Fortunately, the analytic estimates become dominated

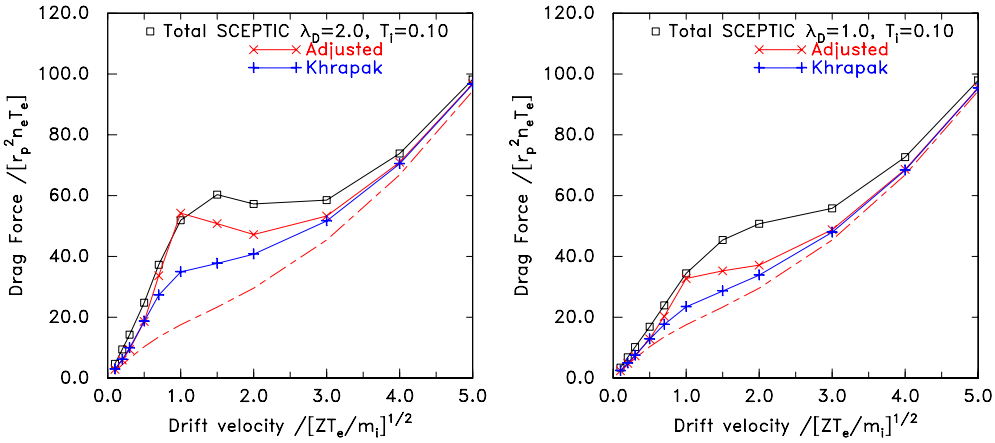

Figure 13. Force comparisons for lower Debye length ($m/Z = 1$: H^+).

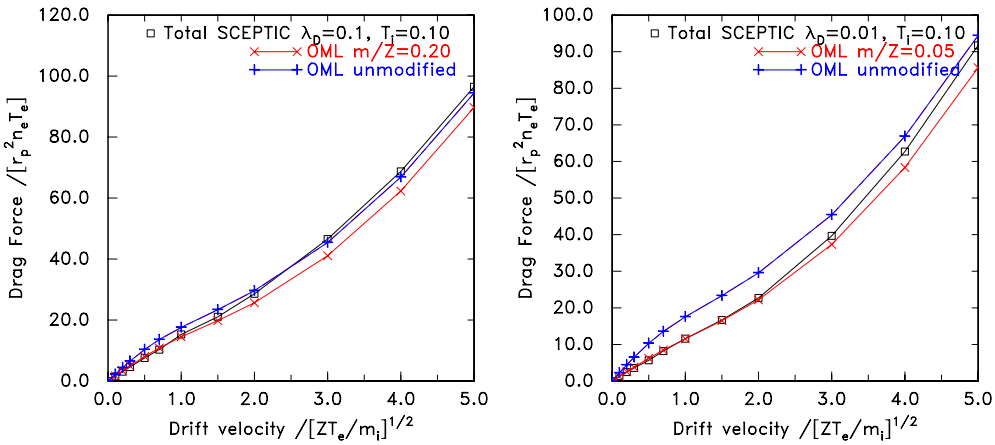

Figure 14. Comparison of the results at $\lambda_{De} \ll r_p$ ($m/Z = 1$: H^+) with the unmodified OML expression (+), which is dominated by F_c, and with an expression in which F_c is based on the modified OML potential ($\times$) given by equation (12).

by the collection force, and the orbital force F_o quickly becomes negligible for $\lambda_{De} < r_p$. Then the analytic expressions rise above the SCEPTIC results because the OML collection flux (8) (which governs the particle potential) is larger than the actual flux, because of the presence of effective potential barriers [19] at intermediate radii. The error in the OML potential partially compensates the OML force error when both are used in the estimates. But as figure 14 shows, the unmodified force obtained by ignoring these errors (which is evaluated here using the plain Khrapak expression since adjustments to F_o are irrelevant) is too large by up to 50% at $\lambda_{De} = 0.1r_p$ and 80% at $\lambda_{De} = 0.01r_p$. If, instead, the drag corresponding to a neutral gas is used (i.e. ignoring the electric field, putting $\chi = 0$ in equation (1)), as several authors have done [20–22], the resulting force is far smaller than the actual force, by factors as large as 7 at low v_f. The neutral approximation is always seriously in error, and should not be used, because it ignores the presheath fields.

In the regime $\lambda_{De} \ll r_p$, there is a separation of length scales between the sheath (thickness $\sim 4\lambda_{De}$) and the presheath ($\sim r_p$) [23]. Essentially all ions that enter the sheath are collected

and the OML treatment can reasonably be applied only to the presheath. An OML collection estimate should therefore be based not on the grain potential but on the potential at the sheath–presheath transition: the sheath edge. In the limit of the zero Debye length, the sheath edge potential is -0.5 to $-1 \times T_e$, sufficient to accelerate the ion fluid to the sound speed, to satisfy the Bohm condition. This potential is substantially smaller in magnitude than the solution of equation (8). One way to interpolate the transition to this new situation is to regard the OML collection force calculation using equation (1) as being governed by an *effective* OML potential that is less negative than that given by substituting actual parameters into (8). This less negative effective potential can be obtained by solving (8) with an artificially lowered effective ion to electron mass ratio m/Z. As illustrated in figure 14, it is found that numerical agreement with SCEPTIC calculations (done with actual $m/Z = 1$), within typically 10% for $\lambda_{De} < 0.2 r_p$, is obtained by adopting for the effective value

$$(m/Z)_{eff} = \max([m/Z]\min(1., 2\lambda_{De}),\ 0.05). \tag{12}$$

This expression reduces the effective OML potential magnitude as λ_{De} drops below 0.5, terminating at a potential of approximately -1 at very small λ_{De}. Of course, it might be appropriate to approximate the collection force at low λ_{De} using expressions based on the ion collection flux calculated by approaches other than OML. The approach embodied in equation (12), though convenient and heuristically motivated, is therefore a tentative proposal, which might not be appropriate for other parameter regimes (e.g. very low ion temperature).

5. Summary

Prior analytic approximations, based on the heuristic adjustments to the Coulomb logarithm integral and the fits to collision cross-sections for Yukawa potentials do not provide accurate values of the collisionless ion drag force when $\lambda_{De} \lesssim 20 r_p$, at low ion temperature. The full-scale simulations of SCEPTIC show complicated and more abrupt transitions of the ion shielding as the flow velocity rises towards the sound speed. The cause of these effects, and of the previously reported reversal of ion collection flux asymmetry and other observed features of the results, has been traced to details of the ion orbits. The abruptness of the transition is largely due to the asymmetric potential: absent from prior approximations.

Equations (1), (2), (4), (10) and (11) provide analytic expressions for the ion drag force. Together with the solution of the OML equations (8) for the floating potential, they can be used to provide convenient and validated values of the drag force, accurate to about 10–20% over the range of relevant ion temperatures and velocities when $\lambda_{De} \geqslant 5 r_p$.

For short Debye length, this analytic approximation still gives reasonable values for the force, which becomes dominated by F_c. However, the effective OML collection potential magnitude must be reduced to represent the formation of the sheath. Using an artificial modification of the mass ratio (equation (12)) in the floating condition is a convenient way to implement that reduction and gives good agreement with the calculated force for $T_i = 0.1 Z T_e$ down to at least $\lambda_{De} = 0.01 r_p$.

Thus, an approximate analytic formula for ion drag force, validated against the SCEPTIC calculations, has been presented, which has useful accuracy over the entire practical range of λ_{De}. Of course, we should recall again that these calculations are for collisionless ions and for idealized ion-absorbing floating grains. The results might be modified in experiments by the effect of collisions or additional charging mechanisms.

Acknowledgments

I am grateful for the incisive comments of the referee. The SCEPTIC calculations were performed on the Alcator Beowulf cluster which is supported by the US DOE grant DE-FC02-99ER54512.

References

[1] Hutchinson I H 2002 *Plasma Phys. Control. Fusion* **44** 1953
[2] Hutchinson I H 2003 *Plasma Phys. Control. Fusion* **45** 1477
[3] Hutchinson I H 2005 *Plasma Phys. Control. Fusion* **47** 71
[4] Chandrasekhar S 1943 *Astrophys. J.* **97** 255
[5] Barnes M S, Keller J H, Forster J C, O'Neill J A and Coultas D K 1992 *Phys. Rev. Lett.* **68** 313
[6] Nitter T 1996 *Plasma Sources Sci. Technol.* **5** 93
[7] Shukla P K and Mamun A A 2002 *Introduction to Dusty Plasma Physics* (Bristol: Institute of Physics Publishing)
[8] Mott-Smith H M and Langmuir I 1926 *Phys. Rev.* **28** 727
[9] Uglov A A and Gnedovets A G 1991 *Plasma Chem. Plasma Process.* **11** 251
[10] Khrapak S A, Ivlev A V, Morfill G E and Thomas H M 2002 *Phys. Rev.* E **66** 046414
[11] Khrapak S A, Ivlev A V, Morfill G E and Zhdanov S D 2003 *Phys. Rev. Lett.* **90** 225002
[12] Khrapak S A, Ivlev A V, Zhdanov S K and Morfill G E 2005 *Phys. Plasmas* **12** 042308
[13] Hahn H-S, Mason E A and Smith F J 1971 *Phys. Fluids* **14** 278
[14] Kilgore M D, Daugherty J E, Porteous R K and Graves D B 1993 *J. Appl. Phys.* **11** 7195
[15] Hutchinson I H 2005 *New Vistas in Dusty Plasmas* ed L Boufendi, M Mikikian and P Shukla, AIP Conference Proceedings (New York: AIP) vol 799, pp 38
[16] Khrapak S A, Ivlev A V, Morfill G E, Zhdanov S K and Thomas H M 2004 *IEEE Trans. Plasma Sci.* **32** 555
[17] Daugherty J E, Porteous R K, Kilgore M D and Graves D B 1992 *J. Appl. Phys.* **72** 3934
[18] Peter T and Meyer-ter Vehn J 1991 *Phys. Rev.* A **43** 1998
[19] Bernstein I B and Rabinowitz I 1959 *Phys. Fluids* **2** 112
[20] Draine B T and Salpeter E E 1979 *Astrophys. J.* **231** 77
[21] Morfill G E *et al* 1980 *Planet. Space Sci.* **28** 1087
[22] Northrop T G 1992 *Phys. Scr.* **45** 475
[23] Hutchinson I H 2002 *Principles of Plasma Diagnostics* (Cambridge: Cambridge University Press) 2nd edn